

ARTICLE



<https://doi.org/10.1038/s41467-021-27104-y>

OPEN

A crystalline radical cation derived from Thiele's hydrocarbon with redox range beyond 1 V

Ying Kai Loh¹, Petra Vasko², Caitilín McManus¹, Andreas Heilmann¹, William K. Myers¹ & Simon Aldridge¹✉

Thiele's hydrocarbon occupies a central role as an open-shell platform for new organic materials, however little is known about its redox behaviour. While recent synthetic approaches involving symmetrical carbene substitution of the CPh₂ termini yield isolable neutral/dicationic analogues, the intervening radical cations are much more difficult to isolate, due to narrow compatible redox ranges (typically < 0.25 V). Here we show that a hybrid BN/carbene approach allows access to an unsymmetrical analogue of Thiele's hydrocarbon **1**, and that this strategy confers markedly enhanced stability on the radical cation. **1**^{•+} is stable across an exceptionally wide redox range (> 1 V), permitting its isolation in crystalline form. Further single-electron oxidation affords borenium dication **1**²⁺, thereby establishing an organoboron redox system fully characterized in all three redox states. We perceive that this strategy can be extended to other transient organic radicals to widen their redox stability window and facilitate their isolation.

¹Inorganic Chemistry Laboratory, Department of Chemistry, University of Oxford, South Parks Road, Oxford OX1 3QR, UK. ²Department of Chemistry, Nanoscience Center, University of Jyväskylä, P. O. Box 35 Jyväskylä FI-40014, Finland. ✉email: simon.aldridge@chem.ox.ac.uk

Shortly after Gomberg's pioneering discovery of the persistent triphenylmethyl radical in 1900¹, Thiele reported the first stable organic diradicaloid ("Thiele's hydrocarbon"; Fig. 1)², derived from *p*-quinodimethane. Thiele's hydrocarbon, which can attain aromaticity in its central ring, can be described by both closed-shell quinoidal (Kekulé) and open-shell diradical (non-Kekulé) resonance forms, accounting for its inherently high reactivity. Subsequently, its X-ray structure was determined, confirming its diradicaloid character³. Since then, Thiele's hydrocarbon has been widely exploited and integrated into the design of new organic materials with small HOMO–LUMO energy gaps⁴.

Organic molecules that can reversibly access three stable redox states have received considerable recent attention^{5–14}, reflecting applications as super-electron donors¹⁵, photo-/electrocatalysts¹⁶, redox switches¹⁷, or in redox-flow batteries etc¹⁸. However, such systems are rarely isolated, due to the redox instability of the intervening radical species¹³. Thiele's hydrocarbon, which can gain aromaticity upon successive one-electron oxidations, presents itself as a privileged platform for such applications. However, its redox properties are far less studied, restricted by the transient nature of its radical monocation ($t_{1/2} = 3$ s), and structural information for both its mono- and dication are unknown (Fig. 1)¹⁹.

Carbenes have recently emerged as highly efficient ligands to stabilize organic radicals^{20–27}, and have granted access to simple non-annulated versions of Thiele's hydrocarbon (Method A, Fig. 1)^{28–31}. This strategy contrasts with traditional (synthetically

challenging) approaches which necessitate the use of multiple planar-fused π -conjugated rings to facilitate spin delocalization⁴. Importantly, the diverse library of available carbenes also allows for modular tuning of the CPh₂ termini³². That said, recently reported analogues based on N-heterocyclic carbenes (NHCs) by Ghadwal et al., cyclic (alkyl)(amino)carbenes (CAACs) and acyclic diaminocarbenes (ADCs) by Jana et al. are characterized either by two single-electron transfer events at potentials which are very close ($\Delta E < 0.25$ V)^{28,29}, or by a single two-electron redox wave^{30,31}, alluding to the instability of the respective mixed-valence radical cations towards disproportionation^{13,33}. As such, these systems are typically limited to only two stable redox states, *viz.* the neutral and dicationic forms. Most recently, Jana et al. pushed this strategy further, reporting that symmetrical CH(NDippMe) disubstitution accesses a more stable radical cation with a redox range extended to 0.48 V³⁴.

Main group heteroatoms have been introduced to modify the electronic properties of π -conjugated organic molecules^{35,36}, leading to the synthesis of silicon³⁷, mono-/dianionic boron^{38,39}, and dicationic nitrogen analogues of Thiele's hydrocarbon⁴⁰. In regards to anionic boron analogues, three-state redox systems have been reported very recently, but the redox ranges associated with the intermediate radicals are also very narrow ($\Delta E = 0.20$ V), thus limiting the stability of these radicals.

An attractive strategy to incorporate boron while still maintaining charge neutrality is to exploit the isoelectronic B=N/C=C relationship⁴¹. Interestingly, this approach has recently been shown to enhance the electronic coupling in electron-rich olefins, leading to isolable olefin radical cations, albeit at the expense of decreasing the stability of the dicationic species, meaning that a three-state redox system could not be achieved⁴². In the context of systems based on Thiele's hydrocarbon, replacement of *both* exocyclic C=C double bonds with B=N successfully delivers isolable BN analogues, as reported by the groups of Piers, Yamashita and Ye (Method B, Fig. 1)^{43–46}. However, in stark contrast to their all-carbon counterparts, these bis-BN analogues are only stable in their *neutral* states. Cyclic voltammetry reveals irreversible one-electron oxidations, hinting at the generation of extremely reactive radical cations and dications derived from these systems that contain a pair of highly electron-deficient boron atoms.

Inspired by these reports, we hypothesized that an unsymmetrical mono-BN analogue of Thiele's hydrocarbon featuring isoelectronic NHC and N-heterocyclic boryl (NHB)^{47–54} substituents might allow access to an isolable radical cation with a significantly enhanced redox range, within an overall three-state system (Method A + B, Fig. 1). Importantly, B=N substitution (Method B) would be expected to render the intervening radical cation stable across a wide redox range by disfavoring the second oxidation step (*cf.* bis-BN systems), albeit moderated somewhat by the presence of the opposing NHC function (Method A) which would mitigate the enhanced electrophilicity at boron in the doubly oxidized dication⁵⁵.

Results and discussion

Syntheses of neutral organoboron analogues of Thiele's hydrocarbon. The large steric profile inherent in both triflate-substituted borane (HCDippN)₂BOTf and IDipp leads to the formation of a B/C frustrated Lewis pair (FLP) system (Fig. 2a)⁵⁶. Upon exposure to pyridine at room temperature, a red solution was formed instantly, implying the facile nature of the 1,4-activation of pyridine. Subsequent deprotonation affords **1** as an orange-red solid; the ¹H NMR spectrum displays two sets of heterocycle signals, consistent with the unsymmetrical environment of opposing NHB and NHC moieties. The boron atom of

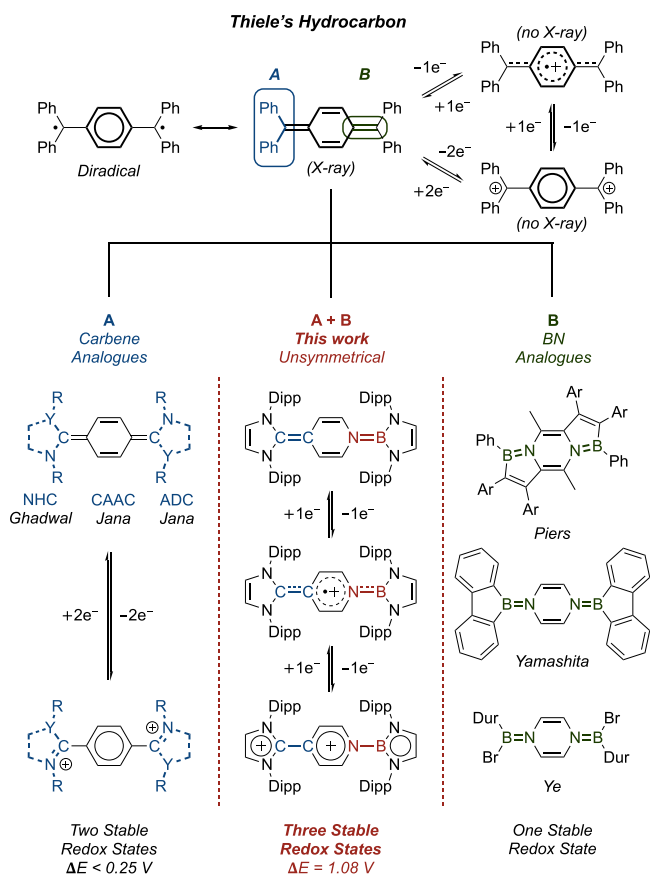


Fig. 1 Systems derived from Thiele's hydrocarbon. Thiele's hydrocarbon, its radical cation and dication; previous modification methods **A**, **B** and present work. (Dipp = 2,6-diisopropylphenyl, NHC = N-heterocyclic carbene, CAAC = cyclic (alkyl)aminocarbenes, ADC = acyclic diaminocarbenes).

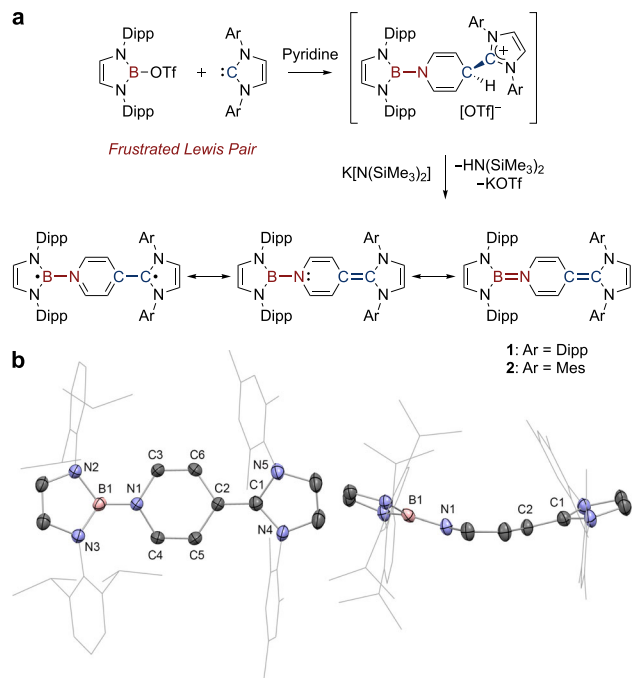


Fig. 2 Syntheses and characterization of neutral organoboron analogues of Thiele's hydrocarbon. **a** Syntheses of **1** and **2**. **b** Solid-state structure of **2** with side view. For clarity, H atoms are omitted, and Dipp/Mes groups are simplified as wireframes. Thermal ellipsoids set at 50% probability. Key distances (Å): B1–N1 1.424(4), C1–C2 1.356(4), N1–C3 1.415(4), N1–C4 1.413(3), C3–C6 1.325(4), C4–C5 1.334(4), C2–C6 1.460(4), C2–C5 1.447(4). (Mes = 2,4,6-trimethylphenyl).

the NHB unit displays a broad signal at 19.9 ppm in the $^{11}\text{B}\{^1\text{H}\}$ NMR spectrum. However, single crystals of **1** gave weak diffraction patterns, and an X-ray structure could not be obtained. As a surrogate for **1**, we synthesized IMes-containing **2** via the same procedure. **2** gives rise to a similar ^{11}B NMR signal (at $\delta_{\text{B}} = 19.0$ ppm), and in this case crystallographic study unambiguously confirms the identity of **2** (and provides credence to **1**) as the target unsymmetrical organoboron analogue of Thiele's hydrocarbon.

Structurally, **2** adopts a curved shape (Fig. 2b). The exocyclic B–N bond (1.424(4) Å) is shorter than the endocyclic B–N bonds (mean: 1.445(4) Å), consistent with a degree of double bond character, and the exocyclic C–C bond (1.356(4) Å) is slightly shorter than those of Thiele's hydrocarbon and related bis-carbene derivatives (1.365(4)–1.381(3) Å)^{3,28–31}. DFT analyses of **1** and **2** show no significant geometric deviations between them and confirm the closed-shell nature of their ground states implied spectroscopically, in line with symmetrical bis-carbene and bis-BN analogues^{28–31,43–46}. In the case of **1**, the calculated singlet-triplet gap is calculated to be 1.76 eV (169.4 kJ mol⁻¹). Moreover, consideration of the natural bond orders obtained from NRT (natural resonance theory) calculations, suggests that the predominant resonance structure features exocyclic B–N single and C=C double bonds (Fig. 2a and Supporting Information Table S4). The localization of a lone pair at nitrogen implied by this resonance structure is consistent with the curved structure of **2**¹².

Cyclic voltammetry was used to elucidate the redox properties of **1**, revealing two reversible single-electron oxidations, consistent with the targeted three-state redox nature (Fig. 3a). The first oxidation wave ($E_1 = -1.47$ V) falls within the range of bis-carbene systems (–1.42 to –0.95 V; Fig. 1)^{28–31}, suggesting that **1**

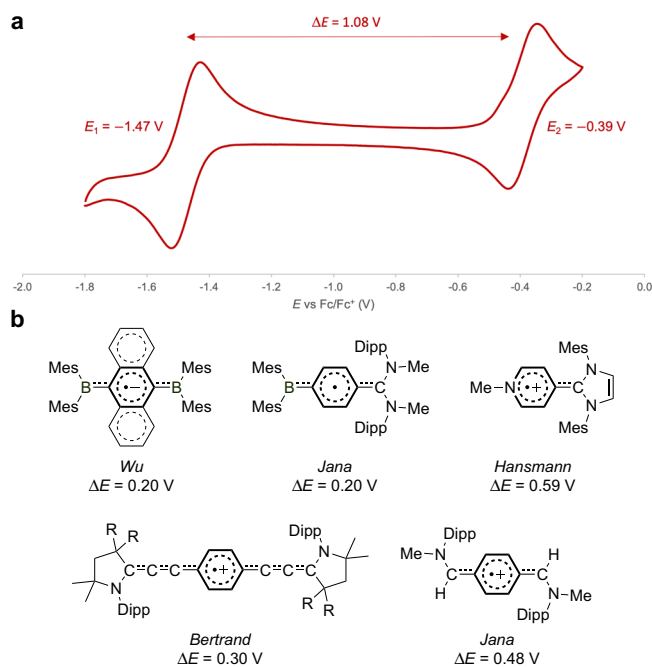


Fig. 3 Electrochemical studies. **a** Cyclic voltammogram of **1** ($[\text{P}^{\text{Bu}}\text{Bu}_4\text{N}][\text{PF}_6]$) in CH_2Cl_2 at 100 mV s^{-1} . **b** Redox ranges associated with related structurally characterized radicals (Hansmann et al. reported in ref. ¹² that a related radical cation $[(\text{MeCMesN})_2\text{C}(\text{C}_5\text{H}_4\text{N})\text{Trip}]^{+\bullet}$ has redox range $\Delta E = 0.72$ V, but this species has not been structurally characterized).

shares similarly strong reducing properties to its all-carbon congeners. Strikingly, the second oxidation wave ($E_2 = -0.39$ V) occurs at a much more positive potential, leading to a markedly wider separation ($\Delta E = 1.08$ V) between the two redox events.

The redox range associated with radical cation $\mathbf{1}^{+\bullet}$ not only greatly exceeds that of the elusive radical cations of bis-carbene analogues ($\Delta E < 0.25$ V; Fig. 1)^{28–31} but also other related structurally characterized radicals ($\Delta E = 0.20$ – 0.59 V; Fig. 3b)^{10,12,34,38,39}, hinting at a pronounced degree of radical stability conferred by BN-substitution. Notably, $\mathbf{1}^{+\bullet}$ can also be viewed as a hybrid of the boryl- C_6H_4 -carbene radical ($\Delta E = 0.20$ V)³⁹ reported by Jana et al. and the pyridyl-carbene radical cation ($\Delta E = 0.59$ V)¹² reported by Hansmann et al. — both of which exhibit much narrower redox ranges independently.

Synthesis of a radical cationic organoboron analogue of Thiele's hydrocarbon. With this in mind, the cationic mono-radical species, $\mathbf{1}^{+\bullet}$, was targeted on a preparative scale by chemical oxidation. Treatment of **1** with $\text{Ag}[\text{SbF}_6]$ (1 equiv.) results in the immediate formation of an NMR-silent dark-brown solution (Fig. 4a). X-ray crystallography confirms its identity as the target mixed-valence radical cation $\mathbf{1}^{+\bullet}[\text{SbF}_6]$ (Fig. 4b). Mono-nuclear boron radical cations are an extremely rare class of boron radical species^{57–59}, in sharp contrast to their neutral and anionic counterparts⁶⁰, presumably due to a confluence of the strong electrophilicity of a boron cation and the high reactivity of an open-shell species. Hence, $\mathbf{1}^{+\bullet}$ represents a rare example of an isolable boron-containing radical cation.

EPR analysis of $\mathbf{1}^{+\bullet}$ (which is in good agreement with simulation) confirms the presence of an unpaired electron centred at $g = 2.0021$, which exhibits hyperfine couplings to B1 [$a(^{11}\text{B}) = 3.32$ G], N1 [$a(^{14}\text{N}) = 3.14$ G], N2'/N3' [$a(^{14}\text{N}) = 2.25$ G] and C3H/C4H [$a(^1\text{H}) = 3.18$ G], hinting at the fully delocalized nature of the radical across the entire π system

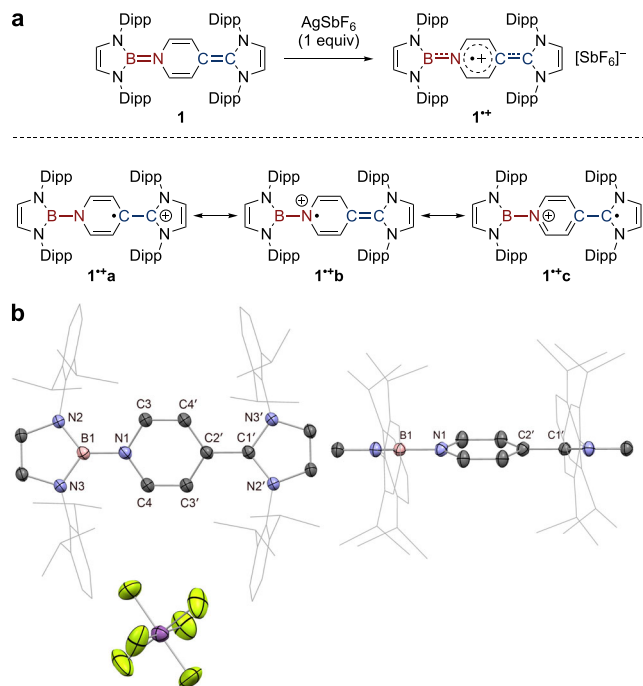


Fig. 4 Synthesis and characterization of radical cationic organoboron analogue of Thiele's hydrocarbon. **a** Synthesis of $1^{+\bullet}$, showing contributing resonance structures. **b** Solid-state structure of $1^{+\bullet}[\text{SbF}_6]^-$ with side view. For clarity, H atoms are omitted and Dipp groups are simplified as wireframes. Thermal ellipsoids set at 50% probability. Key distances (Å): B1–N1 1.465(4), C1'–C2' 1.465(4), N1–C3 1.407(4), N1–C4 1.397(4), C3–C4' 1.363(4), C3'–C4 1.363(4), C2'–C4' 1.397(4), C2'–C3' 1.407(4).

(Fig. 5a). Interestingly, the ^{11}B hyperfine coupling constant (3.32 G) is larger than for diborene radical cations (< 1.18 G)^{61,62}, and in the range of mononuclear boron radical cations (2.10 – 6.43 G)^{57–59}, suggesting boron radical character in $1^{+\bullet}$.

Spin-density analysis confirms the delocalized picture, with a significant contribution on the central pyridyl ring (65%; Fig. 5b). Informatively, the spin population across the B=N (15%) bond is lower than the C=C (27%) bond, reflecting the more localized nature of the B=N (as opposed to C=C) bridge and resulting in an unsymmetrical distribution of the remaining spin density from the central ring onto the peripheral NHB (6%) and NHC (27%) ligands. As such, $1^{+\bullet}$ can be described by several contributing resonance forms (Fig. 4a): (i) C-centred pyridyl radical $1^{+\bullet\text{a}}$; (ii) N-centred pyridyl radical $1^{+\bullet\text{b}}$; and (iii) NHC-centred radical $1^{+\bullet\text{c}}$. Contributions from these three resonance structures account for (i) the majority of the unpaired spin density being located on the pyridyl and NHC heterocycles; and (ii) for NRT-derived natural bond order data for $1^{+\bullet}$ which shows reduced bond order alternation in the central pyridyl ring compared to **1** (but greater than in 1^{2+} , see below), and an exocyclic C–C bond order which is also between those determined for **1** and 1^{2+} . It is also noteworthy that in metal-free radical borylations catalyzed by 4-substituted pyridines, a pyridine-stabilized boryl radical has been invoked as the key reactive intermediate^{63–65}. $1^{+\bullet}$ can be regarded as a crystalline analogue of this boryl radical species.

Synthesis of a dicationic organoboron analogue of Thiele's hydrocarbon. Completion of the redox triad was accomplished by synthesis of the corresponding dication. Treatment of **1** with $\text{Ag}[\text{SbF}_6]$ (2 equiv.) results in successive colour changes from deep red to dark brown and ultimately to a persistent deep purple solution (Fig. 6a). The product is NMR-active and the ^1H

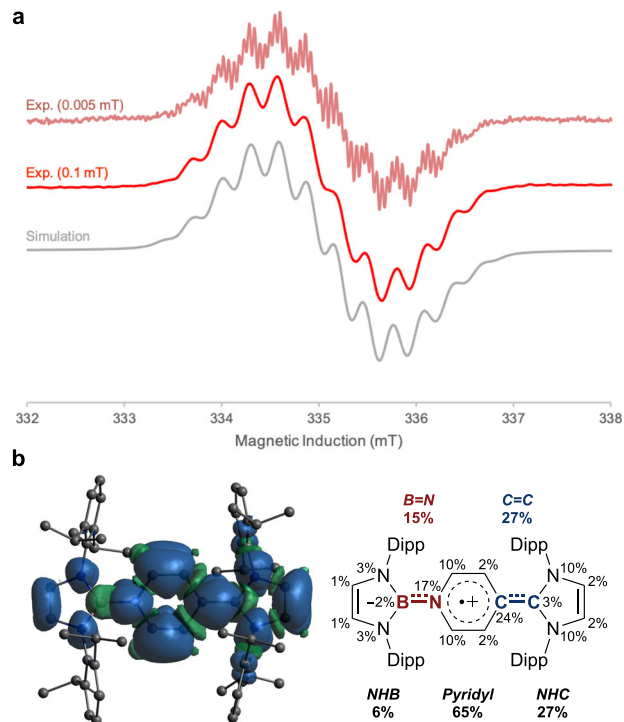


Fig. 5 EPR studies. **a** Experimental EPR spectra at indicated field modulations (red) and simulation (grey) of $1^{+\bullet}$, detailed in SI. **b** Calculated spin density. The negative spin densities ($\rho(\alpha) - \rho(\beta) < 0$), at the boron atom are the result of spin polarization of underlying orbitals by the SOMO. The polarization effect on s-character orbitals results in large Fermi-contact hyperfine interactions. A spatial difference in α and β orbitals leads to a change in the overall spin-density sign.

spectrum reveals a marked downfield shift of the pyridyl ring protons, suggesting increased aromaticity within the central ring, while the boron signal of the NHB unit is essentially unchanged ($\delta_{\text{B}} = 20.1$ ppm). X-ray crystallography confirms its identity as the target doubly oxidized dication $1^{2+}[\text{SbF}_6]_2$ (Fig. 6b). Three-coordinate borenium dications are extremely rare^{66,67}, and no further redox chemistry has been reported for the isolated systems, possibly due to the presence of strongly π -donating ligands tailor-made to stabilize these highly electron-deficient species^{68–70}. Hence, 1^{2+} together with $1^{+\bullet}$ and **1** constitutes an isolable organoboron redox triad which can reversibly shuttle between dicationic, radical cationic and neutral states.

With regard to 1^{2+} , NPA analysis reveals the two positive charges to be highly delocalized, with boron bearing the greatest share of positive charge (+0.94). This value is larger than that determined for bis(carbodicarbene)[BH]²⁺ system (+0.36) reported by Ong et al.⁶⁶, but close to that of bis(imino)[BPh]²⁺ dication (+1.02) reported by Inoue et al.⁶⁷. As such, 1^{2+} can also be described by several contributing resonance forms (Fig. 6a): (i) pyridinium–imidazolium $1^{2+\text{a}}$; (ii) borenium–imidazolium $1^{2+\text{b}}$; or (iii) borenium dication $1^{2+\text{c}}$. NICS calculations are consistent with the aromatic character of the central ring suggested by the NMR measurements (NICS(0) = -7.55 ; NICS(1) = -8.99), and contrast with the non-aromatic character for $1^{+\bullet}$ (NICS(0) = 1.52; NICS(1) = -0.87) and anti-aromatic character for **1** (NICS(0) = 6.67, NICS(1) = 4.14). Moreover, the natural bond orders obtained from NRT calculations (Supporting Information Table S4), suggest that $1^{2+\text{a}}$ / $1^{2+\text{b}}$ represent the overwhelmingly dominant resonance structures (exocyclic B–N/C–C single bonds; equivalent bonds within the central heterocycle).

In the solid state, both $1^{+\bullet}$ and 1^{2+} sit on a crystallographic inversion centre (Figs. 4b and 6b). Hence, the BN- and CC-

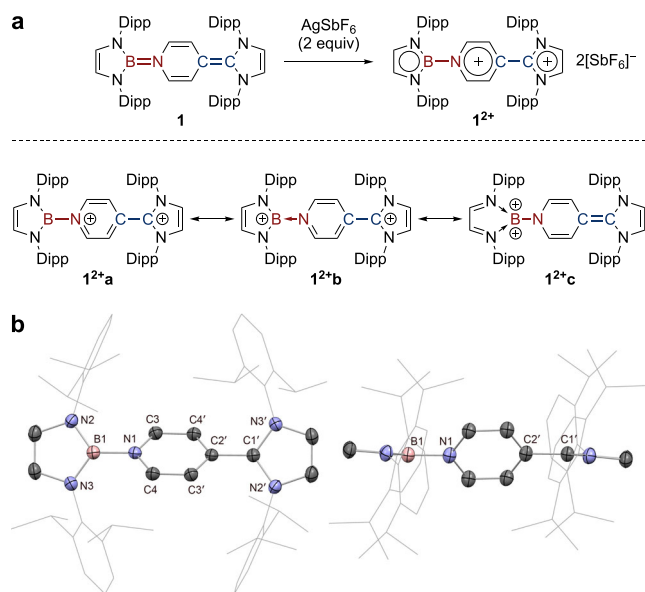


Fig. 6 Synthesis and characterization of dicationic organoboron analogue of Thiele's hydrocarbon. **a** Synthesis of 1^{2+} , showing contributing resonance structures. **b** Solid-state structure of $1^{2+}[\text{SbF}_6]_2$ with side view. For clarity, $[\text{SbF}_6]^-$ counter-anions and H atoms omitted, Dipp groups simplified as wireframes. Thermal ellipsoids set at 50% probability. Key distances (\AA): B1–N1 1.495(3), C1'–C2' 1.495(3), N1–C3 1.367(3), N1–C4 1.374(3), C3–C4' 1.375(3), C3'–C4 1.375(3), C2'–C4' 1.374(3), C2'–C3' 1.367(3).

containing halves in each structure are modelled as identical fragments, and geometric discussions of 1^{+} and 1^{2+} are based upon the mean values for each. Upon successive single-electron oxidations, the exocyclic B–N and C–C linkages lengthen, with accompanying reduction of the bond length alternation (BLA) in the pyridyl ring, consistent with diminishing exocyclic double-bond character and concomitant aromaticity enhancement (Table 1). This is also reflected in the progressive twisting of the central ring away from coplanarity with the peripheral NHB and NHC ligands.

The UV–vis spectra (and associated TD-DFT calculations) show a gradual red-shifting of the prominent absorption bands from **1** ($\lambda_{\text{max}} = 342 \text{ nm}$; HOMO \rightarrow LUMO+9) to 1^{+} ($\lambda_{\text{max}} = 442 \text{ nm}$; SOMO(β) \rightarrow LUMO(β)) to 1^{2+} ($\lambda_{\text{max}} = 537 \text{ nm}$; HOMO \rightarrow LUMO) upon successive one-electron oxidations (Fig. 7). Interestingly, the very broad absorption band of 1^{2+} (range: 400–700 nm) arising from the charge transfer from the NHB ligand to the central pyridyl ring, stretches across the visible region. This is in contrast to dications derived from wholly carbon systems which are typically restricted to absorptions in the UV region^{6–13}, and hints at potential applications of all three states of this organoboron redox system in visible light photoredox catalysis.

To conclude, we disclose an unsymmetrical organoboron analogue of Thiele's hydrocarbon **1**, derived from isoelectronic NHB and NHC ligands. We demonstrate that B=N substitution confers an electronic coupling enhancement of $> 1 \text{ V}$, enabling the isolation of a boron-containing radical cation 1^{+} related to Thiele's hydrocarbon. Further single-electron oxidation affords borenium dication 1^{2+} , thereby establishing a new organoboron reversible redox triad featuring **1**, 1^{+} and 1^{2+} . We propose that formal BN/CC substitution is critical in lowering the energy of the LUMO of the dication 1^{2+} (see Supporting Information, Fig. S19) compared to its all-carbon analogue, making 1^{2+} more oxidizing, and rendering the intermediate radical cation 1^{+} less prone to oxidation than its neutral counterpart **1**¹³. This

Table 1 Mean distances (\AA) and angles ($^\circ$) between BN- and CC-containing fragments (DFT-calculated exocyclic bond lengths given in square parentheses).

	B1–N1/C1'–C2'	BLA (pyridyl)	Twist (pyridyl)
2	1.430(4), 1.356(4)	0.072(4)	10.7
1^{+}	1.465(4) [1.469, 1.416]	0.029(4)	16.4
1^{2+}	1.495(3) [1.499, 1.453]	0.005(3)	46.7

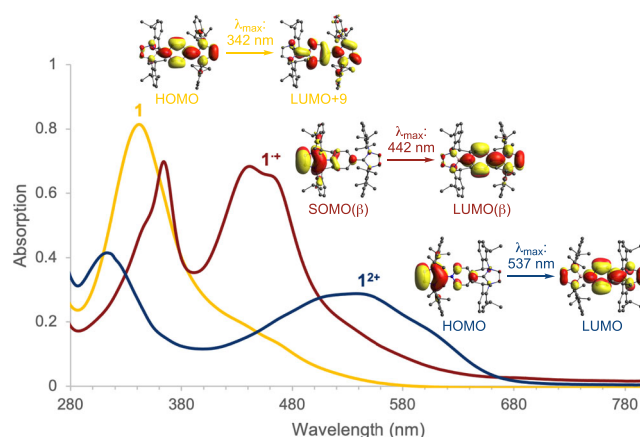


Fig. 7 UV-vis studies. UV-vis spectra of **1**, 1^{+} and 1^{2+} in CH_2Cl_2 ; key absorption assignments by TD-DFT.

hypothesis accounts for the stability of 1^{+} over an unprecedented redox range, and is consistent with the experimental observation that dicationic species derived from doubly BN-substituted systems (Fig. 1, Method B) are too oxidizing to be experimentally accessible. As such, we perceive that our present strategy can be extended to other transient organic radicals to imbue maximal stability and facilitate their isolation.

Methods

General considerations. All manipulations were carried out using standard Schlenk line or dry-box techniques under an atmosphere of argon or dinitrogen. Solvents were degassed by sparging with argon and dried by passing through a column of the appropriate drying agent. NMR spectra were measured in benzene- d_6 (which was dried over potassium), with the solvent then being distilled under reduced pressure and stored under argon in Teflon valve ampoules. NMR samples were prepared under argon in 5 mm Wilmad 507-PP tubes fitted with J. Young Teflon valves. ^1H , $^{13}\text{C}\{^1\text{H}\}$, $^{11}\text{B}\{^1\text{H}\}$, $^{19}\text{F}\{^1\text{H}\}$ NMR spectra were recorded on Bruker Avance III HD nanobay 400 MHz or Bruker Avance 500 MHz spectrometer at ambient temperature and referenced internally to residual protio-solvent (^1H) or solvent (^{13}C) resonances and are reported relative to tetramethylsilane ($\delta = 0 \text{ ppm}$). ^{19}F resonances are referenced externally to CFCl_3 . Assignments were confirmed using two-dimensional ^1H - ^1H and ^{13}C - ^1H NMR correlation experiments. Chemical shifts are quoted in δ (ppm) and coupling constants in Hz. Elemental analyses were carried out by London Metropolitan University. $(\text{HCDippN})_2\text{BBr}$ was prepared by the literature method (see Supplementary Information S1). All other reagents were used as received.

Preparation of $(\text{HCDippN})_2\text{BOTf}$. To a mixture of $(\text{HCDippN})_2\text{BBr}$ (2.00 g, 4.28 mmol) and AgOTf (1.65 g, 6.42 mmol) was added CHCl_3 (3 mL) and stirred for 3 days at 60°C in an ampoule. To the suspension was added benzene (20 mL) and filtered. The filtrate was dried under vacuum to yield a solid covered in a tar-like substance. To this was added *n*-hexane (250 mL) and benzene (10 mL) to dislodge the tar-like substance and filtered. The filtrate was dried under vacuum to yield $(\text{HCDippN})_2\text{BOTf}$ (1.08 g, 47% yield) as a greyish-green powder. ^1H NMR (400 MHz, C_6D_6 , 297 K): $\delta = 1.16$ (d, $^3J_{\text{HH}} = 6.9 \text{ Hz}$, 12H, $\text{CH}(\text{CH}_3)_2$), 1.33 (d, $^3J_{\text{HH}} = 6.9 \text{ Hz}$, 12H, $\text{CH}(\text{CH}_3)_2$), 3.16 (sept, $^3J_{\text{HH}} = 6.9 \text{ Hz}$, 4H, $\text{CH}(\text{CH}_3)_2$), 6.01 (s, 2H, NCH), 7.10–7.12 (m, 4H, Dipp-*m*-CH), 7.18–7.22 (m, 2H, Dipp-*p*-CH); $^{11}\text{B}\{^1\text{H}\}$ NMR (128 MHz, C_6D_6): $\delta = 19.0$; $^{19}\text{F}\{^1\text{H}\}$ NMR (377 MHz, C_6D_6): $\delta = -76.68$. **Elemental analysis** calculated for $\text{C}_{27}\text{H}_{36}\text{BF}_3\text{N}_2\text{O}_5\text{S}$: C 60.45%, H 6.76%, N 5.22%, found: C 60.11%, H 6.55%, N 4.98%.

Preparation of 1. To a mixture of (HCDippN)₂BOTf (200 mg, 0.37 mmol) and (HCDippN)₂C (145 mg, 0.37 mmol) in benzene (1 mL) was added pyridine (0.1 mL, 1.24 mmol) and stirred for 5 min at room temperature to form a red solution. To the solution was added K[N(SiMe₃)₂] (75 mg, 0.38 mmol) at room temperature and stirred for 5 min at room temperature to form a deep red solution. Volatiles were removed under vacuum. To the residue was added benzene (5 mL) and the mixture filtered. The filtrate was dried under vacuum to yield **1** (264 mg, 83% yield) as an orange-red powder. ¹H NMR (500 MHz, C₆D₆, 297 K): δ = 1.18 (t, ³J_{HH} = 6.6 Hz, 24H, CH(CH₃)₂), 1.30 (d, ³J_{HH} = 6.9 Hz, 12H, CH(CH₃)₂), 1.35 (d, ³J_{HH} = 6.9 Hz, 12H, CH(CH₃)₂), 3.27 (sept, ³J_{HH} = 6.9 Hz, 4H, CH(CH₃)₂), 3.38 (sept, ³J_{HH} = 6.9 Hz, 4H, CH(CH₃)₂), 4.14 (d, ³J_{HH} = 8.6 Hz, 2H, Py-CH), 4.81 (d, ³J_{HH} = 8.6 Hz, 2H, Py-CH), 5.61 (s, 2H, NCH), 5.80 (s, 2H, NCH), 6.95 (d, ³J_{HH} = 7.6 Hz, 4H, Dipp-*m*-CH), 7.01–7.08 (m, 8H, Dipp-*CH*); ¹³C{¹H} NMR (126 MHz, C₆D₆): δ = 23.3 (CH(CH₃)₂), 23.7 (CH(CH₃)₂), 24.5 (CH(CH₃)₂), 24.7 (CH(CH₃)₂), 28.7 (CH(CH₃)₂), 81.5 (Py-*p*-C), 107.6 (Py-CH), 117.3 (NCH), 118.5 (NCH), 121.1 (Py-CH), 123.6 (Dipp-*m*-CH), 123.9 (Dipp-*m*-CH), 127.6 (Dipp-*p*-CH), 128.7 (Dipp-*p*-CH), 132.4 (NCN), 137.7 (Dipp-*i*-C), 139.8 (Dipp-*i*-C), 146.3 (Dipp-*o*-C), 147.7 (Dipp-*o*-C); ¹¹B{¹H} NMR (128 MHz, C₆D₆): δ = 19.9; UV-vis (CH₂Cl₂, λ_{max}): 342 nm (ε = 16284 M⁻¹cm⁻¹).

Preparation of 2. To a mixture of (HCDippN)₂BOTf (200 mg, 0.37 mmol) and (HCDippN)₂C (114 mg, 0.37 mmol) in benzene (1 mL) was added pyridine (0.1 mL, 1.24 mmol) and stirred for 5 min at room temperature to form a red solution. To the solution was added K[N(SiMe₃)₂] (75 mg, 0.38 mmol) at room temperature and stirred for 5 min at room temperature to form a deep red solution. Volatiles were removed under vacuum. To the residue was added *n*-hexane (25 mL) and the mixture filtered. The filtrate was dried under vacuum to yield **2** (159 mg, 56% yield) as an orange-red powder. Single crystals (yellow plates) suitable for X-ray crystallography were obtained by slow evaporation of a concentrated solution of **2** in *n*-pentane at room temperature. ¹H NMR (500 MHz, C₆D₆, 297 K): δ = 1.20 (d, ³J_{HH} = 6.9 Hz, 12H, CH(CH₃)₂), 1.29 (d, ³J_{HH} = 6.9 Hz, 12H, CH(CH₃)₂), 2.07 (s, 6H, Mes-*p*-CCH₃), 2.21 (s, 12H, Mes-*o*-CCH₃), 3.32 (sept, ³J_{HH} = 6.9 Hz, 4H, CH(CH₃)₂), 4.28 (d, ³J_{HH} = 8.4 Hz, 2H, Py-CH), 4.92 (d, ³J_{HH} = 8.4 Hz, 2H, Py-CH), 5.47 (s, 2H, NCH), 5.83 (s, 2H, NCH), 6.57 (s, 4H, Mes-*m*-CH), 6.99–7.01 (m, 4H, Dipp-*CH*), 7.05–7.08 (m, 2H, Dipp-*CH*); ¹³C{¹H} NMR (126 MHz, C₆D₆): δ = 18.4 (Mes-*o*-CCH₃), 21.0 (Mes-*p*-CCH₃), 23.6 (CH(CH₃)₂), 24.7 (CH(CH₃)₂), 28.7 (CH(CH₃)₂), 81.5 (Py-*p*-C), 107.6 (Py-CH), 116.3 (NCH), 118.4 (NCH), 121.4 (Py-CH), 123.6 (Dipp-*m*-CH), 127.6 (Dipp-*p*-CH), 129.3 (Mes-*m*-CH), 131.2 (NCN), 136.5 (Mes-*p*-C), 136.6 (Mes-*o*-C), 136.9 (Mes-*i*-C), 140.0 (Dipp-*i*-C), 146.3 (Dipp-*o*-C); ¹¹B{¹H} NMR (128 MHz, C₆D₆): δ = 20.5; **Elemental analysis** calculated for C₅₂H₆₄BN₅: C 81.12%, H 8.38%, N 9.10%, found: C 80.91%, H 8.20%, N 8.89%.

Preparation of [1][SbF₆]. To a mixture of **1** (300 mg, 0.35 mmol) and AgSbF₆ (121 mg, 0.35 mmol) was added CH₂Cl₂ (3 mL) and stirred for 5 min at room temperature to form a dark-brown solution. The mixture was filtered and the filtrate was dried under vacuum to yield [1][SbF₆] (325 mg, 85% yield) as a dark-brown powder. Single crystals (brown rods and plates) suitable for X-ray crystallography were obtained by slow evaporation of a concentrated solution of [1][SbF₆] in fluorobenzene at room temperature. **X-band EPR** g = 2.0021 (1xB: -9.3 MHz; 1xN_{py}: 8.8 MHz; 2xN_{IDipp}: 6.3 MHz; 2xH_{Py-*o*-CH}: -8.9 MHz); UV-vis (CH₂Cl₂, λ_{max}): 364 nm (ε = 13983 M⁻¹cm⁻¹), 442 nm (ε = 13682 M⁻¹cm⁻¹); **Elemental analysis** calculated for C₅₈H₇₆BF₆N₅Sb: C 63.92%, H 7.03%, N 6.43%, found: C 63.77%, H 7.13%, N 6.29%.

Preparation of [1][SbF₆]₂. To a mixture of **1** (50 mg, 0.06 mmol) and AgSbF₆ (40 mg, 0.12 mmol) was added CH₂Cl₂ (2 mL) and stirred for 5 min at room temperature to form a deep purple solution. The mixture was filtered and the filtrate was dried under vacuum to yield [1][SbF₆]₂ (43 mg, 56% yield) as a purple powder. Single crystals (purple rods) suitable for X-ray crystallography were obtained by slow evaporation of a concentrated solution of [1][SbF₆]₂ in CH₂Cl₂ at room temperature. ¹H NMR (400 MHz, CD₂Cl₂, 297 K): δ = 0.85 (d, ³J_{HH} = 6.9 Hz, 12H, CH(CH₃)₂), 0.91 (d, ³J_{HH} = 6.8 Hz, 12H, CH(CH₃)₂), 1.17 (d, ³J_{HH} = 6.8 Hz, 12H, CH(CH₃)₂), 1.22 (d, ³J_{HH} = 6.7 Hz, 12H, CH(CH₃)₂), 2.21 (sept, ³J_{HH} = 6.8 Hz, 4H, CH(CH₃)₂), 2.66 (sept, ³J_{HH} = 6.8 Hz, 4H, CH(CH₃)₂), 6.56 (s, 2H, NCH), 7.14 (d, ³J_{HH} = 7.2 Hz, 2H, Py-CH), 7.27 (d, ³J_{HH} = 7.8 Hz, 4H, Dipp-*m*-CH), 7.38 (d, ³J_{HH} = 7.9 Hz, 4H, Dipp-*m*-CH), 7.47 (t, ³J_{HH} = 7.8 Hz, 2H, Dipp-*p*-CH), 7.69 (t, ³J_{HH} = 7.9 Hz, 2H, Dipp-*p*-CH), 7.97 (d, ³J_{HH} = 7.2 Hz, 2H, Py-CH), 8.03 (s, 2H, NCH); ¹³C{¹H} NMR (126 MHz, CD₂Cl₂): δ = 22.7 (CH(CH₃)₂), 23.4 (CH(CH₃)₂), 25.2 (CH(CH₃)₂), 25.5 (CH(CH₃)₂), 29.1 (CH(CH₃)₂), 29.9 (CH(CH₃)₂), 122.7 (NCH), 125.6 (Dipp-*m*-CH), 126.8 (Dipp-*m*-CH), 127.3 (Py-CH), 128.8 (Dipp-*i*-C), 130.1 (NCN), 130.6 (Dipp-*p*-CH), 133.4 (Dipp-*i*-C), 134.4 (Dipp-*p*-CH), 137.3 (Py-*p*-C), 137.4 (NCH), 144.7 (Dipp-*o*-C), 145.3 (Py-CH), 145.4 (Dipp-*o*-C); ¹¹B{¹H} NMR (128 MHz, CD₂Cl₂): δ = 20.1; UV-vis (CH₂Cl₂, λ_{max}): 313 nm (ε = 8294 M⁻¹cm⁻¹), 537 nm (ε = 5756 M⁻¹cm⁻¹); **Elemental analysis** for C₅₈H₇₆BF₁₂N₅Sb₂: C 52.55%, H 5.78%, N 5.28%, found: C 52.63%, H 5.51%, N 5.30%.

Data availability

The crystallographic data generated in this study have been deposited in the CCDC structural database under accession codes 2063252-2063254 [www.ccdc.cam.ac.uk].

Spectroscopic data are available in the Supplementary Information and through the Oxford Research Archive (www.ora.ox.ac.uk).

Received: 8 June 2021; Accepted: 3 November 2021;

Published online: 03 December 2021

References

- Gomberg, M. An instance of trivalent carbon: triphenylmethyl. *J. Am. Chem. Soc.* **22**, 757–771 (1900).
- Thiele, J. & Balhorn, H. Ueber einen chinoïden kohlenwasserstoff. *Ber. Dtsch. Chem. Ges.* **37**, 1463–1470 (1904).
- Montgomery, L. K., Huffman, J. C., Jurczak, E. A. & Grendze, M. P. The molecular structures of Thiele's and Chichibabin's hydrocarbons. *J. Am. Chem. Soc.* **108**, 6004–6011 (1986).
- Chen, Z. X., Li, Y. & Huang, F. Persistent and stable organic radicals: design, synthesis, and applications. *Chem* <https://doi.org/10.1016/j.chempr.2020.09.024> (2020).
- Deuchert, K. & Hünig, S. Multistage organic redox systems—a general structural principle. *Angew. Chem. Int. Ed. Engl.* **17**, 875–886 (1978).
- Li, Y. et al. C₄ Cumulene and the corresponding air-stable radical cation and dication. *Angew. Chem. Int. Ed.* **53**, 4168–4172 (2014).
- Jin, L., Melaimi, M., Liu, L. & Bertrand, G. Singlet carbenes as mimics for transition metals: synthesis of an air-stable organic mixed valence compound [M₂(C₂)⁺⁺; M = cyclic(alkyl)(amino)carbene]. *Org. Chem. Front.* **1**, 351–354 (2014).
- Munz, D., Chu, J., Melaimi, M. & Bertrand, G. NHC-CAAC heterodimers with three stable oxidation states. *Angew. Chem. Int. Ed.* **55**, 12886–12890 (2016).
- Hansmann, M. M., Melaimi, M., Munz, D. & Bertrand, G. Modular approach to Kekulé diradicaloids derived from cyclic (alkyl)(amino)carbenes. *J. Am. Chem. Soc.* **140**, 2546–2554 (2018).
- Hansmann, M. M., Melaimi, M. & Bertrand, G. Organic mixed valence compounds derived from cyclic (alkyl)(amino)carbenes. *J. Am. Chem. Soc.* **140**, 2206–2213 (2018).
- Antoni, P. W. & Hansmann, M. M. Pyrylenes: a new class of tunable, redox-switchable, photoexcitable pyrylium–carbene hybrids with three stable redox-states. *J. Am. Chem. Soc.* **140**, 14823–14835 (2018).
- Antoni, P. W., Bruckhoff, T. & Hansmann, M. M. Organic redox systems based on pyridinium–carbene hybrids. *J. Am. Chem. Soc.* **141**, 9701–9711 (2019).
- Messelberger, J. et al. Aromaticity and sterics control whether a cationic olefin radical is resistant to disproportionation. *Chem. Sci.* **11**, 4138–4149 (2020).
- Freeman, L. A. et al. Soluble, crystalline, and thermally stable alkali CO₂⁻ and carbonate (CO₃²⁻) clusters supported by cyclic (alkyl)(amino) carbenes. *Chem. Sci.* **12**, 3544–3550 (2021).
- Broggi, J., Terme, T. & Vanelle, P. Organic electron donors as powerful single-electron reducing agents in organic synthesis. *Angew. Chem. Int. Ed.* **53**, 384–413 (2014).
- Romero, N. A. & Nicewicz, D. A. Organic photoredox catalysis. *Chem. Rev.* **116**, 10075–10166 (2016).
- Schröder, H. V. & Schalley, C. A. Tetrathiafulvalene—a redox-switchable building block to control motion in mechanically interlocked molecules. *Beilstein J. Org. Chem.* **14**, 2163–2185 (2018).
- Luo, J., Hu, B., Hu, M., Zhao, Y. & Liu, T. L. Status and prospects of organic redox flow batteries toward sustainable energy storage. *ACS Energy Lett.* **4**, 2220–2240 (2019).
- Hart, H., Fleming, J. S. & Dye, J. L. One-electron transfer from an olefin to a dicarbonium ion. *J. Am. Chem. Soc.* **86**, 2079–2080 (1964).
- Kato, K. & Osuka, A. Platforms for stable carbon-centered radicals. *Angew. Chem. Int. Ed.* **58**, 8978–8986 (2019).
- Kundu, S., Sinhababu, S., Chandrasekhar, V. & Roesky, H. W. Stable cyclic (alkyl)(amino)carbene (CAAC) radicals with main group substituents. *Chem. Sci.* **10**, 4727–4741 (2019).
- Ghadwal, R. S. Stable carbon-centered radicals based on N-heterocyclic carbenes. *Synlett* **30**, 1765–1775 (2019).
- Nesterov, V. et al. NHCs in main group chemistry. *Chem. Rev.* **118**, 9678–9842 (2018).
- Kim, Y. & Lee, E. Stable organic radicals derived from N-heterocyclic carbenes. *Chem. Eur. J.* **24**, 19110–19121 (2018).
- Melaimi, M., Jassar, R., Soleilhavoup, M. & Bertrand, G. Cyclic (alkyl)(amino)carbenes (CAACs): recent developments. *Angew. Chem. Int. Ed.* **56**, 10046–10068 (2017).
- Soleilhavoup, M. & Bertrand, G. Cyclic (alkyl)(amino)carbenes (CAACs): stable carbenes on the rise. *Acc. Chem. Res.* **48**, 256–266 (2015).
- Martin, C. D., Soleilhavoup, M. & Bertrand, G. Carbene-stabilized main group radicals and radical ions. *Chem. Sci.* **4**, 3020–3030 (2013).

28. Rottschäfer, D. et al. N-Heterocyclic carbene analogues of Thiele and Chichibabin hydrocarbons. *Angew. Chem. Int. Ed.* **57**, 5838–5842 (2018).
29. Rottschäfer, D., Neumann, B., Stammler, H.-G., Andrada, D. M. & Ghadwal, R. S. Kekulé diradicaloids derived from a classical N-heterocyclic carbene. *Chem. Sci.* **9**, 4970–4976 (2018).
30. Maiti, A. et al. CAAC based Thiele and Schlenk hydrocarbon. *Angew. Chem. Int. Ed.* **59**, 6729–6734 (2020).
31. Maiti, A., Chandra, S., Sarkar, B. & Jana, A. Acyclic diaminocarbene-based Thiele, Chichibabin, and Müller hydrocarbons. *Chem. Sci.* **11**, 11827–11833 (2020).
32. Melaimi, M., Soleilhavou, M. & Bertrand, G. Stable cyclic carbenes and related species beyond diaminocarbenes. *Angew. Chem. Int. Ed.* **49**, 8810–8849 (2010).
33. Hankache, J. & Wenger, O. S. Organic mixed valence. *Chem. Rev.* **111**, 5138–5178 (2011).
34. Mahata, A. et al. α,α' -Diamino-*p*-quinodimethanes with three stable oxidation states. *Org. Lett.* **22**, 8332–8336 (2020).
35. Loh, Y. K. & Aldridge, S. Acid–base free main group carbonyl analogues. *Angew. Chem. Int. Ed.* **60**, 8626–8648 (2021).
36. Fischer, R. C. & Power, P. P. π -Bonding and the lone pair effect in multiple bonds involving heavier main group elements: developments in the new millennium. *Chem. Rev.* **110**, 3877–3923 (2010).
37. Nozawa, T., Nagata, M., Ichinohe, M. & Sekiguchi, A. Isolable *p*- and *m*-[(Bu_2MeSi) $_2\text{Si}$] $_2\text{C}_6\text{H}_4$: disilaquinodimethane vs triplet bis(silyl radical). *J. Am. Chem. Soc.* **133**, 5773–5775 (2011).
38. Zheng, Y., Xiong, J., Sun, Y., Pan, X. & Wu, J. Stepwise reduction of 9,10-bis(dimesitylboryl)anthracene. *Angew. Chem. Int. Ed.* **54**, 1293–12936 (2015).
39. Maiti, A. et al. Anionic boron- and carbon-based hetero-diradicaloids spanned by a *p*-phenylene bridge. *J. Am. Chem. Soc.* **143**, 3687–3692 (2021).
40. Su, Y. et al. Nitrogen analogues of Thiele's hydrocarbon. *Angew. Chem. Int. Ed.* **54**, 1634–1637 (2015).
41. Campbell, P. G., Marwitz, A. J. V. & Liu, S.-Y. Recent advances in azaborine chemistry. *Angew. Chem. Int. Ed.* **51**, 6074–6092 (2012).
42. Su, Y., Li, Y., Ganguly, R. & Kinjo, R. Crystalline boron-linked tetraaminoethylene radical cations. *Chem. Sci.* **8**, 7419–7423 (2017).
43. Morgan, M. M. et al. Zirconocene-based methods for the preparation of BN-indenes: application to the synthesis of 1, 5-dibora-4a, 8a-diaza-1, 2, 3, 5, 6, 7-hexaaryl-4, 8-dimethyl-s-indacenes. *Organometallics* **36**, 2541–2551 (2017).
44. Noguchi, M. et al. Planar and bent BN-embedded *p*-quinodimethanes synthesized by transmetalation of bis(trimethylsilyl)-1,4-dihydropyrazines with chloroborane. *Organometallics* **37**, 1833–1836 (2018).
45. Katsuma, Y., Asakawa, H. & Yamashita, M. Reactivity of highly Lewis acidic diborane(4) towards pyridine and isocyanide: formation of boraalkene–pyridine complex and ortho- functionalized pyridine derivatives. *Chem. Sci.* **9**, 1301–1310 (2018).
46. Ma, L. et al. Reactions of dihaloboranes with electron-rich 1,4-bis(trimethylsilyl)-1,4-diaza-2,5-cyclohexadienes. *Molecules* **25**, 2875 (2020).
47. Weber, L. Recent progress in 1,3,2-diazaborole chemistry. *Coord. Chem. Rev.* <https://doi.org/10.1016/j.ccr.2020.213667> (2021).
48. Stephan, D. W. A tale of two elements: the Lewis acidity/basicity umpolung of boron and phosphorus. *Angew. Chem. Int. Ed.* **56**, 5984–5992 (2017).
49. Protchenko, A. V. et al. Stable GaX₂, InX₂ and TlX₂ radicals. *Nat. Chem.* **6**, 315–319 (2014).
50. Asami, S., Ishida, S., Iwamoto, T., Suzuki, K. & Yamashita, M. Isolation and characterization of radical anions derived from a boryl-substituted diphosphene. *Angew. Chem. Int. Ed.* **56**, 1658–1662 (2017).
51. Schröder, J. et al. Isolation of a stable pyridine radical anion. *Chem. Commun.* **55**, 1322–1325 (2019).
52. Loh, Y. K., Ying, L., Fuentes, M. Á., Do, D. C. H. & Aldridge, S. An N-heterocyclic boryloxy ligand isoelectronic with N-heterocyclic imines: access to an acyclic dioxysilylene and its heavier congeners. *Angew. Chem. Int. Ed.* **58**, 4847–4851 (2019).
53. Loh, Y. K. et al. An acid-free anionic oxoborane isoelectronic with carbonyl: facile access and transfer of a terminal B=O double bond. *J. Am. Chem. Soc.* **141**, 8073–8077 (2019).
54. Helling, C., Cutsail, G. E. III, Weinert, H., Wölper, C. & Schulz, S. Ligand effects on the electronic structure of heteroleptic antimony-centered radicals. *Angew. Chem. Int. Ed.* **59**, 7561–7568 (2020).
55. Loh, Y. K., Fuentes, M. Á., Vasko, P. & Aldridge, S. Successive protonation of an N-heterocyclic imine derived carbonyl: superelectrophilic dication versus masked acylium ion. *Angew. Chem. Int. Ed.* **57**, 16559–16563 (2018).
56. Stephan, D. W. The broadening reach of frustrated Lewis pair chemistry. *Science* **354**, aaf7229 (2016).
57. Kinjo, R., Donnadiou, B., Celik, M. A., Frenking, G. & Bertrand, G. Synthesis and characterization of a neutral tricoordinate organoboron isoelectronic with amines. *Science* **333**, 610–613 (2011).
58. Sarkar, S. K. et al. Isolation of base stabilized fluoroborylene and its radical cation. *Dalton Trans.* **48**, 8551–8555 (2019).
59. Suzuki, S., Yoshida, K., Kozaki, M. & Okada, K. Syntheses and structural studies of tris(N-phenothiazinyl)borane and its radical cation. *Angew. Chem. Int. Ed.* **52**, 2499–2502 (2013).
60. Su, Y. & Kinjo, R. Boron-containing radical species. *Coord. Chem. Rev.* **352**, 346–378 (2017).
61. Bissinger, P. et al. Boron radical cations from the facile oxidation of electron-rich diborenes. *Angew. Chem. Int. Ed.* **53**, 5689–5693 (2014).
62. Bissinger, P. et al. Boron as a powerful reductant: synthesis of a stable boron-centered radical-anion radical-cation pair. *Angew. Chem. Int. Ed.* **54**, 359–362 (2015).
63. Liu, L. L. & Stephan, D. W. Radicals derived from Lewis acid/base pairs. *Chem. Soc. Rev.* **48**, 3454–3463 (2019).
64. Frieze, F. W. & Studer, A. New avenues for C–B bond formation via radical intermediates. *Chem. Sci.* **10**, 8503–8518 (2019).
65. Wang, G. et al. Homolytic cleavage of a B–B bond by the cooperative catalysis of two Lewis bases: computational design and experimental verification. *Angew. Chem. Int. Ed.* **55**, 5985–5989 (2016).
66. Chen, W.-C. et al. The elusive three-coordinate dicationic hydrido boron complex. *J. Am. Chem. Soc.* **136**, 914–917 (2014).
67. Franz, D., Szilvási, T., Pöthig, A., Deiser, F. & Inoue, S. Three-coordinate boron(III) and diboron(II) dications. *Chem. Eur. J.* **24**, 4283–4288 (2018).
68. Franz, D. & Inoue, S. Cationic complexes of boron and aluminum: an early 21st century viewpoint. *Chem. Eur. J.* **25**, 2898–2926 (2019).
69. Lin, Y. & Chiu, C. Mono- and polynuclear boron dications. *Chem. Lett.* **46**, 913–922 (2017).
70. Piers, W. E., Bourke, S. C. & Conroy, K. C. Borinium, borenium, and boronium ions: synthesis, reactivity, and applications. *Angew. Chem. Int. Ed.* **44**, 5016–5036 (2005).

Acknowledgements

We would like to thank A*STAR (scholarship for Y.K.L.), EPSRC (EP/V036408/1 and EP/L011972/1 for The Centre for Advanced ESR (CAESR); scholarship for C.Mc.M.), the Leverhulme Trust (RP-2018-246), Academy of Finland (project number 314794, P.V.).

Author contributions

Y.K.L. conceived and performed the synthetic experiments. P.V. conducted theoretical analysis and CV experiments. C.Mc.M. and A.H. collected and solved the X-ray structures. W.M. conducted EPR studies. S.A. supervised the study. The manuscript is written by Y.K.L. and S.A.

Competing interests

The authors declare no competing interests.

Additional information

Supplementary information The online version contains supplementary material available at <https://doi.org/10.1038/s41467-021-27104-y>.

Correspondence and requests for materials should be addressed to Simon Aldridge.

Peer review information *Nature Communications* thanks Liu Liu and the other, anonymous, reviewer(s) for their contribution to the peer review of this work. Peer reviewer reports are available.

Reprints and permission information is available at <http://www.nature.com/reprints>

Publisher's note Springer Nature remains neutral with regard to jurisdictional claims in published maps and institutional affiliations.



Open Access This article is licensed under a Creative Commons Attribution 4.0 International License, which permits use, sharing, adaptation, distribution and reproduction in any medium or format, as long as you give appropriate credit to the original author(s) and the source, provide a link to the Creative Commons license, and indicate if changes were made. The images or other third party material in this article are included in the article's Creative Commons license, unless indicated otherwise in a credit line to the material. If material is not included in the article's Creative Commons license and your intended use is not permitted by statutory regulation or exceeds the permitted use, you will need to obtain permission directly from the copyright holder. To view a copy of this license, visit <http://creativecommons.org/licenses/by/4.0/>.

© The Author(s) 2021